

Single-Pore versus Dual-Pore Bipyridine-Based Covalent–Organic Frameworks: An Insight into the Heterogeneous Catalytic Activity for Selective C–H Functionalization

Harsh Vardhan, Abdullah M. Al-Enizi, Ayman Nafady, Yanxiong Pan, Zhongyu Yang, Humberto R. Gutiérrez, Xiaolong Han, and Shengqian Ma*

Exponential growth in the field of covalent–organic frameworks (COFs) is emanating from the direct correlation between designing principles and desired properties. The comparison of catalytic activity between single-pore and dual-pore COFs is of importance to establish structure–function relationship. Herein, the synthesis of imine-linked dual-pore [(BPYDC)]_{x%}-ETTA COFs (x = 0%, 25%, 50%, 75%, 100%) with controllable bipyridine content is fulfilled by three-component condensation of 4,4',4'',4'''-(ethene-1,1,2,2-tetrayl)tetraaniline (ETTA), 4,4'-biphenyldialdehyde, and 2,2'-bipyridyl-5,5'-dialdehyde in different stoichiometric ratio. The strong coordination of bipyridine moieties of [(BPYDC)]_{x%}-ETTA COFs with palladium imparts efficient catalytic active sites for selective functionalization of sp² C–H bond to C–X (X = Br, Cl) or C–O bonds in good yield. To broaden the scope of regioselective C–H functionalization, a wide range of electronically and sterically substituted substrates under optimized catalytic condition are investigated. A comparison of the catalytic activity of palladium decorated dual-pore frameworks with single-pore imine-linked Pd(II)@Py-2,2'-BPYDC framework is undertaken. The finding of this work provides a sporadic example of chelation-assisted C–H functionalization and disclosed an in-depth comparison of the relationship between superior catalytic activity and core properties of rationally designed imine linked frameworks.

1. Introduction

The expansion of metal-catalyzed methods for the regio- and chemoselective C–H functionalization of arene and alkane remains a critical challenge in the field of organometallic chemistry.^[1–3] The functionalization of sp² and sp³ C–H bond is well-studied,^[4–9] however, their application in the synthesis of complex organic structure is usually restricted due to the harsh reaction condition, low functional group tolerance, and byproduct formation. C–H to C–O, C–N, C–C, and C–X (X = Cl, Br, I) transformation are fundamental conversions of great importance in the synthesis of natural products, medicinal compounds, and pharmaceuticals.^[10–12] Direct C–H bond functionalization suffers from two core challenges, the inert nature of C–H bond and control site selectivity with diverse C–H groups. In this respect, the work of Sanford and co-workers on chelate-directed C–H functionalization has attracted widespread attention.^[2,13–17] In principle, the regioselective C–H bond oxidation

H. Vardhan, Prof. S. Ma
Department of Chemistry
University of South Florida
4202 E. Fowler Avenue, Tampa, FL 33620, USA


Prof. A. M. Al-Enizi, Prof. A. Nafady
Department of Chemistry
College of Science
King Saud University
Riyadh 11451, Saudi Arabia

Dr. Y. Pan, Prof. Z. Yang
Department of Chemistry and Biochemistry
North Dakota State University
1231 Albrecht Blvd., Fargo, ND 58108, USA

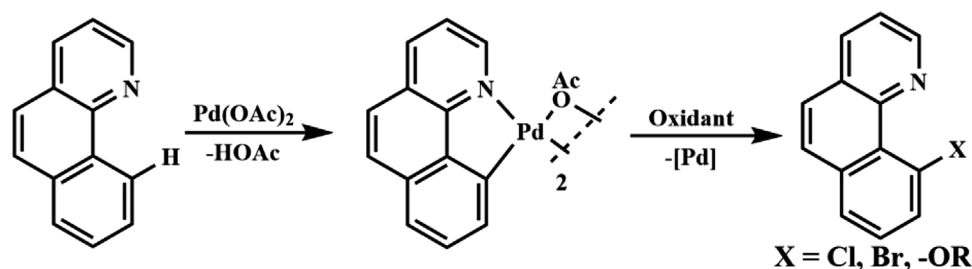
Prof. H. R. Gutiérrez
Department of Physics
University of South Florida
Tampa, FL 33620, USA

Prof. X. Han
School of Chemical Engineering
Northwest University
Xi'an, Shaanxi 710069, China

Prof. S. Ma
Department of Chemistry
University of North Texas
1508 W Mulberry St, Denton, TX 76201, USA
E-mail: Shengqian.Ma@unt.edu

 The ORCID identification number(s) for the author(s) of this article can be found under <https://doi.org/10.1002/smll.202003970>.

DOI: 10.1002/smll.202003970



Scheme 1. Regioselective sp^2 C–H functionalization of benzo[*h*]quinoline.

involves the use of substrates bearing coordinating functional group that bind to metal catalyst and direct oxidation to a specific C–H bond within the substrate. As shown in **Scheme 1**, C–H bond of benzo[*h*]quinoline undergoes cyclopalladation (C–Pd), which is more reactive than C–H counterparts, and induces Pd centers compatibility with range of oxidants such as iodobenzene diacetate thereby enabling many different types of bonds, including C–X (X = Cl, Br, I), C–O, C–N, C–S, C–C with high selectivity.^[18–23] Practically, homogeneous catalytic systems are known to have various drawbacks including lack of recyclability, reusability, and tedious purification steps. However, incorporation of enriched palladium chemistry with covalent–organic frameworks (COFs) can serve as a platform to overcome these shortcomings and expand this exciting research domain.

COFs are an emerging class of porous crystalline materials that allow the integration of functionalized building blocks into networks via range of covalent linkages.^[24–27] The structure–function relationship of frameworks depends on the versatile synthetic strategy, network topology, heterogeneous linker exchange, binding functionalities, and flexible regulation of pore size/volume.^[28–34] The tunability of structural properties along with high surface area, chemical and thermal stability make COFs one of the most promising candidates for catalysis,^[35–39] gas storage/separation,^[40–45] environmental remediation,^[46–48] optoelectronics,^[49–51] energy storage,^[52–55] biomedical,^[56–58] atmospheric water harvesting,^[59] and chemosensor.^[60] The cooperative assistance of pore size, pore shape, and binding sites in the COFs skeleton facilitates docking of catalysts to investigate fundamental organic conversions. Pore surface engineering via immobilization of vanadium, iridium, copper ions in bipyridine, and catechol-functionalized COFs is crucial for a range of catalytic reactions.^[35,61–63] Ni-DBA-2D-COF and Ni-DBA-3D COF provide rare example of Ni(0) binding with π -electron conjugated dehydrobenzoannulene (DBA) motifs.^[64,65] Mono and bimetallic postsynthetic modification of COFs increase catalyst life time and activity, for instance, Rh^I/Pd^{II} COF, corrole COF, and M/Salen-COF serve as reusable catalyst for cascade reactions,^[66] photodynamic therapy,^[67] and Henry reaction,^[68] respectively. In addition, molybdenum-doped COF (Mo-COF) serve as a nanochannel-reactor for cyclohexene epoxidation with 99% conversion and over 70% selectivity.^[69] NUS-50-Co and NUS-51-Co synthesized via impregnation of cobalt in hydroxy-rich hydrazone-based COFs demonstrate catalytic activity for cyanosilylation reaction of electronically and sterically substituted aldehydes.^[70] The chemical modification in COFs tuned the physical and chemical properties of frameworks,^[71,72] for instance, Yaghi and co-workers reported conversion of imine-linked IL COF-1

to oxazole-linked LZU-192 and thiazole-linked COF-921.^[73] In addition, COF-170 undergoes multistep solid-state reactions to afford cyclic carbamate and thiocarbamate-linked framework.^[74] The same group also illustrated amidation, esterification, and thioesterification of COF-616.^[75] Apart from pore surface engineering, de novo strategy was used to synthesize COFs with catalytic building blocks. In this regard, β -ketoenamine linked COFs^[76–78] and BINOL-based COFs^[36] established good catalytic activity for cascade reactions and asymmetric addition reaction of diethylzinc to aldehydes, respectively. Moreover, heterobimetallic Re(I) bipyridine based framework exhibited faraday efficiency of 18(2)% for electrochemical carbon dioxide reduction to carbon monoxide.^[79–81] Recently, the COF-SQ prepared by condensation of 1,3,5-triformylbenzene and 3,4-bis((4-aminophenyl)amino)cyclo-but-3-ene-1,2-dione served as organocatalyst for Michael addition.^[82]

In this contribution, we demonstrate the structure–function relationship in C–H functionalization using palladium decorated imine-linked dual pore, hexagonal and triangular, [(BPyDC)_{*x*}]-ETTA COFs (x = 0%, 25%, 50%, 75%, 100%) with controllable bipyridine contents. The role of fundamental properties on the catalytic efficiency and stability was outlined by comparing with palladium immobilized single-pore imine-linked Pd(II)@Py-2,2'-BPyDC framework. This structure–function relationship provides facile platform for the design of frameworks having better catalytic activity, stability, and recyclability for practically important organic and organometallic conversions.

2. Results and Discussion

In developing structure–function relationship in COFs, a D_{2h} symmetric fourfold amine-functionalized tetraphenylethylene (4,4',4'',4'''-(ethene-1,1,2,2-tetrayl)tetraaniline (ETTA)), with two distinct angles (60° and 120°) between two adjacent arms has been known as a versatile scaffold to construct dual-pore COFs. To induce controllable bipyridine content, [(BPyDC)_{*x*}]-ETTA COFs (x = 0%, 25%, 50%, 75%, 100%) were synthesized by reacting ETTA, 2,2'-bipyridyl-5,5'-dialdehyde (2,2'-BPyDCA), and 4,4'-biphenyldialdehyde (4,4'-BPhDCA) in different stoichiometric ratio using 1,4-dioxane as a solvent in the presence of catalytic amount of 6 M acetic acid (**Figure 1**). Fourier transform infrared (FTIR) spectra of the isolated products confirmed direct imine condensation in [(BPyDC)_{*x*}]-ETTA COFs (x = 0%, 25%, 50%, 75%, 100%) with –CN stretch at 1619 cm^{-1} (Figure S1, Supporting Information). ¹³C cross-polarization magic angle spinning nuclear magnetic resonance (CP-MAS NMR) spectrum

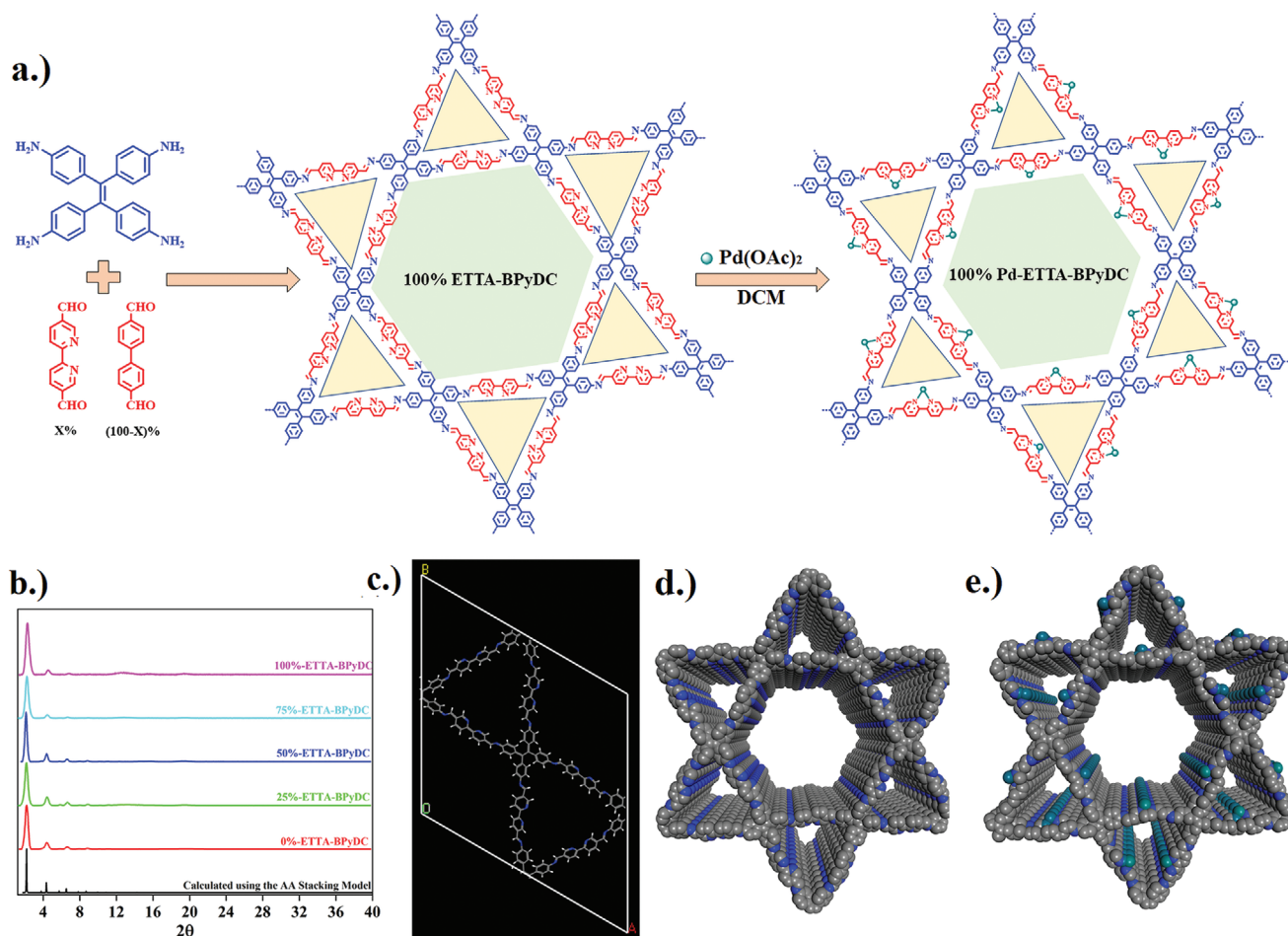


Figure 1. a) Synthetic scheme of $[(\text{BPyDC})_x\%-\text{ETTA}]$ COFs ($x = 0\%$, 25% , 50% , 75% , 100%) through the condensation of 2,2'-bipyridyl-5,5'-dialdehyde (2,2'-BPyDCA), 4,4',4''-(ethene-1,1,2,2-tetrayl)tetraaniline (ETTA), 4,4'-biphenyldialdehyde (4,4'-BPhDCA), and Pd(II) @ $[(\text{BPyDC})_x\%-\text{ETTA}]$ COFs. b) Calculated and experimental PXRD pattern of $[(\text{BPyDC})_x\%-\text{ETTA}]$ COFs ($x = 0\%$, 25% , 50% , 75% , 100%). c) Unit cell of $(\text{BPyDC})_{100\%}-\text{ETTA}$ COF. Graphic extended view of AA-stacking mode of dual-pore framework; d) $(\text{BPyDC})_{100\%}-\text{ETTA}$ COF. e) Pd(II) @ $(\text{BPyDC})_{100\%}-\text{ETTA}$ COF.

exhibited characteristic resonance signal for imine carbon at 157 ppm, which lends further confirmation for the condensation reaction between two precursor units (Figure S2, Supporting Information). Powder X-ray diffraction (PXRD) data were acquired to expound the structure of the as-synthesized frameworks. PXRD pattern of $[(\text{BPyDC})_{100\%}-\text{ETTA}]$ COF revealed strong peak at 2.2° together with relatively weaker peaks at 3.8° , 4.4° , 6.6° , and 19.7° assigned to (100), (110), (200), (300), and (001) diffractions. The experimental PXRD pattern was in a good agreement with the calculated pattern of bipyridine-based framework, which strongly suggests that $[(\text{BPyDC})_{100\%}-\text{ETTA}]$ exhibited dual-pore structure with AA stacking model ($a = b = 47.04 \text{ \AA}$, $c = 4.51 \text{ \AA}$, $\alpha = \beta = 90^\circ$, and $\gamma = 120^\circ$). The similar diffraction patterns were also obtained for $[(\text{BPyDC})_{0\%}-\text{ETTA}]$, $[(\text{BPyDC})_{25\%}-\text{ETTA}]$, $[(\text{BPyDC})_{50\%}-\text{ETTA}]$, and $[(\text{BPyDC})_{75\%}-\text{ETTA}]$ COFs, indicating that bipyridine controlled frameworks demonstrated similar crystallinity (Figure 1b). Micro- and mesoporousity for $[(\text{BPyDC})_x\%-\text{ETTA}]$ COFs ($x = 0\%$, 25% , 50% , 75% , 100%) were investigated by nitrogen adsorption isotherms at 77 K. The Brunauer–Emmett–Teller and Langmuir surface area are summarized in Figures S3 and S4 (Supporting Information),

varying from 663 and $829 \text{ m}^2\text{g}^{-1}$ for 0%-ETTA-BPyDC to 341 and $433 \text{ m}^2\text{g}^{-1}$ for 100%-ETTA-BPyDC COF with triangular and hexagonal pore width of 1.3 nm and 3.1 nm, respectively. Moreover, thermogravimetric analysis (TGA) results revealed high thermal stability of bipyridine controlled frameworks with breakdown temperature of 400°C (Figure S5, Supporting Information), indicating that the framework can be used for pore surface engineering at room and elevated temperatures. Elemental analysis showed that carbon, nitrogen, and hydrogen contents of the $[(\text{BPyDC})_x\%-\text{ETTA}]$ COFs ($x = 0\%$, 25% , 50% , 75% , 100%) were close to the calculated values (Table S1, Supporting Information).

The combined thermal stability, surface area, and dual-pore nature revealed that the bipyridine controlled frameworks could be used as a decorating platform for palladium immobilization to study structure–function relation in C–H functionalization. In doing so, solution-infiltration strategy was employed for palladium immobilization via reaction of $[(\text{BPyDC})_x\%-\text{ETTA}]$ COFs ($x = 0\%$, 25% , 50% , 75% , 100%) with $\text{Pd}(\text{OAc})_2$ at ambient temperature for 12 h (Figure 1). The resulting immobilized frameworks, referred as Pd(II) @ $[(\text{BPyDC})_x\%-\text{ETTA}]$ COFs ($x = 0\%$, 25% , 50% , 75% , 100%), were characterized using

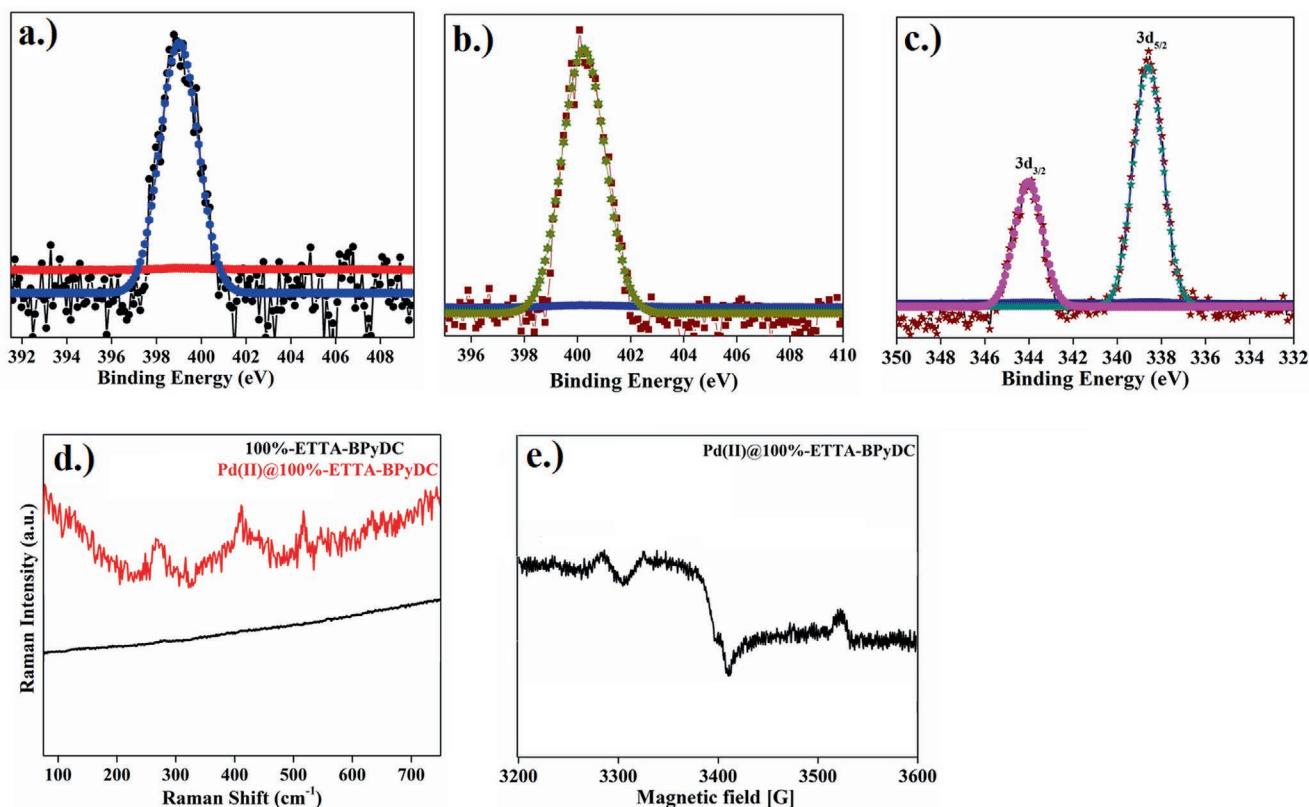


Figure 2. a–c) XPS spectra of 100%-ETTA-BPyDC (nitrogen), Pd(II)@100%-ETTA-BPyDC (nitrogen), and Pd(II)@100%-ETTA-BPyDC (palladium); d) Raman spectrum comparison of 100%-ETTA-BPyDC and Pd(II)@100%-ETTA-BPyDC; e) EPR spectra of Pd(II)@100%-ETTA-BPyDC.

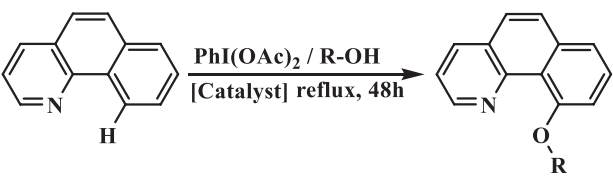
various analytical techniques. Scanning electron microscopy (SEM) images of Pd(II)@(BPyDC)_{x%}-ETTA COFs exhibited plate-like morphology similar to pristine (BPyDC)_{x%}-ETTA COFs. This confirms that immobilization took place on the pores of frameworks rather than reside on the outer surface (Figures S6 and S7, Supporting Information). Energy-dispersive X-ray spectroscopy (EDX) analysis via SEM indicates the presence of palladium in dual-pore immobilized frameworks. Moreover, X-ray photoelectron spectroscopy (XPS) was performed to examine the coordination environment of nitrogen and palladium in docked frameworks. (BPyDC)_{x%}-ETTA COFs ($x = 0\%$, 25%, 50%, 75%, 100%) exhibited a N1s signal at 398.4 eV, which is shifted to higher value of 400.2 eV after palladium immobilization, indicating coordination of palladium to the bipyridine functionalities in Pd(II)@(BPyDC)_{100%}-ETTA (Figure 2a–c). Furthermore, the palladium region peaks for 3d_{3/2} and 3d_{5/2} illustrated the binding energy centered at 343.3 and 337.8 eV, respectively, which is characteristic of divalent Pd ions, thereby eliminating the possibility of any Pd(0) particles.^[83] Similar variation was observed for palladium coordination with bipyridine functionalities of Pd(II)@(BPyDC)_{x%}-ETTA COFs ($x = 25\%$, 50%, 75%) as shown in Figure S8 (Supporting Information). The confirmation of Pd(II)–N linkage in Pd(II)@100%-ETTA-BPyDC was established by Raman spectroscopy, as the symmetric Pd(II)–N stretching vibration is Raman active over the range from 560 to 430 cm⁻¹ (Figure 2d), as compared to peaks in pristine 100%-ETTA-BPyDC framework.^[84] Additionally, the binding of Pd(II) with bipyridine functionalities, similar

to cyclopalladated complexes, was evident from electron paramagnetic resonance (EPR) spectrum as shown in Figure 2e.^[85] FTIR and ¹³C CP-MAS NMR spectra exhibited vibrational band and chemical shift at 1619 cm⁻¹ and 158 ppm, respectively, thus, indicating the complete retention of imine functionalities during postsynthetic modification (Figures S9 and S10). Moreover, the peaks at 179.8 and 23.2 ppm in ¹³C CP-MAS NMR spectrum established the presence of acetate functionalities linked with palladium. Importantly, PXRD pattern showed that there is no substantial difference with respect to the crystalline nature of frameworks during palladium immobilization, while the observed decrease in the relative intensity of Pd(II)@(BPyDC)_{x%}-ETTA COFs ($x = 0\%$, 25%, 50%, 75%, 100%) was probably due to the inclusion of palladium in the pores of the frameworks (Figure S11, Supporting Information).^[35,64,86] This observation was further validated by the N₂ adsorption isotherm of Pd(II)@(BPyDC)_{x%}-ETTA COFs ($x = 0\%$, 25%, 50%, 75%, 100%) at 77 K. As expected, the Brunauer–Emmett–Teller (BET) and Langmuir surface area decrease in comparison to pristine frameworks as summarized in Figure S12 (Supporting Information). In this context, Pd(II)@100%-ETTA-BPyDC shows BET surface area of 198 m² g⁻¹ as compared to 341 m² g⁻¹ for pristine 100%-ETTA-BPyDC. Inductively coupled plasma mass spectrometry (ICP-MS) results revealed that the palladium content in Pd(II)@(BPyDC)_{x%}-ETTA COFs ($x = 25\%$, 50%, 75%, 100%) varies from 2.3 to 5.9 wt%. The TGA profile of immobilized frameworks exhibited sharp weight loss at 324 °C ascribed to the degradation of framework, thereby opens

the opportunities to address catalytic reactions at elevated temperature (Figure S13, Supporting Information).

With coordinatively accessible palladium centers decorated in stable dual-pore COFs, we sought to investigate the catalytic activity in regioselective C–H to C–O and C–X (X = Br, Cl, I) functionalization. Most common methods reported for C–H oxidation either require strong base or strong acids such as $\text{CF}_3\text{SO}_3\text{H}$, $n\text{-BuLi}$.^[87,88] Homogeneous Pd(II)-catalyzed methods for chelate-directed C–H functionalization have been studied in organometallic chemistry and bipyridine COFs can serve as a decorating platform to prepare heterogeneous catalysts that can be recyclable and reusable. The oxidation of benzo[*h*]quinoline (**1**) sp^2 C₁₀–H bond to alkoxy groups using iodobenzene diacetate $[\text{PhI}(\text{OAc})_2]$ as an oxidant was studied in the presence of Pd(II)@(BPyDC)_{*x*%}-ETTA COFs (*x* = 25%, 50%, 75%, 100%). Results showed that the C–H to C–O functionalization does not occur in presence of pristine 100%-BPyDC-ETTA and in absence of any oxidant. However, using Pd(II)@(BPyDC)_{*x*%}-ETTA COFs (*x* = 25%, 50%, 75%, 100%) as catalysts, quantitative yield of methoxy-functionalized **1** was achieved in 48 h at 65 °C (Table 1, entry 3–6), which illustrates the significant role of immobilized palladium framework in catalytic reaction. Presumably, the C–H₁₀ single bond of benzo[*h*]quinoline undergoes cyclopalladation in the presence of immobilized frameworks, followed by treatment with iodobenzene diacetate as an oxidant to attain C–O functionalities. Furthermore, homogeneous Pd(OAc)₂ catalytic system afforded good yield for methoxy-functionalized **1** (Table 1, entry 7) when compared to Pd(II)@100%-ETTA-BPyDC. To further extend the scope of this reaction, we installed a range of alkoxy functional group to form alkyl-aryl ether such as –OEt, –OCH₂CF₃, –O(CH₂)₂CH₃, –O(CH₂)₃CH₃ in good to moderate yields. Interestingly, using

Table 1. Regioselective C–H to C–OR functionalization of benzo[*h*]quinoline using homogeneous and heterogeneous catalysts.



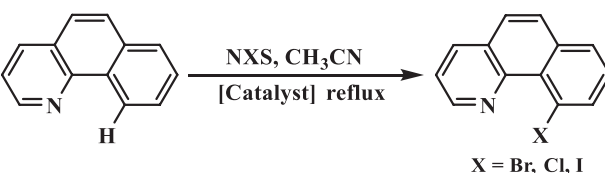
Entry	R (product/solvent)	Catalyst	Yield ^{a)} [%]
1	CH ₃	Blank	0
2 ^{b)}	CH ₃	100%-ETTA-BPyDC	<5
3 ^{b)}	CH ₃	Pd(II)@25%-ETTA-BPyDC	21
4 ^{b)}	CH ₃	Pd(II)@50%-ETTA-BPyDC	49
5 ^{b)}	CH ₃	Pd(II)@75%-ETTA-BPyDC	71
6 ^{b)}	CH ₃	Pd(II)@100%-ETTA-BPyDC	86
7 ^{b)}	CH ₃	Pd(OAc) ₂	97
8 ^{b)}	CH ₂ CH ₃	Pd(II)@100%-ETTA-BPyDC	72
9 ^{b)}	CH ₂ CF ₃	Pd(II)@100%-ETTA-BPyDC	77
10 ^{b)}	(CH ₂) ₂ CH ₃	Pd(II)@100%-ETTA-BPyDC	27
11 ^{b)}	(CH ₂) ₃ CH ₃	Pd(II)@100%-ETTA-BPyDC	<10

^{a)}Determined by ¹H-NMR; ^{b)}0.05 mmol of substrate, 0.125 mmol of $\text{PhI}(\text{OAc})_2$, catalyst (100 mg), and 2.0 mL of alcohol (R–OH).

1-propanol and 1-butanol as solvents yielded lower conversion percentages, probably owing to the weak nucleophilicity of the bulky propoxy and butoxy groups (Table 1, entry 8–11); however, trifluoroethanol may facilitate nucleophilic aromatic substitution, which probably underlines the cause of higher percentage yield as compared to ethanol.^[89] To confirm the heterogeneous nature of Pd(II)@(BPyDC)_{100%}-ETTA COF, a hot filtration reaction was performed after 12 h and removing the catalyst afforded almost no conversion to C–H functionalized product (Figure S14, Supporting Information).

Chelate-directed oxidation can be extended to halogenations using *N*-halosuccinimide (NXS, X = C, B, I) as both oxidant and halogenating reagents. Similar to C–O functionalization, C–Br conversion, i.e., monobromated benzo[*h*]quinoline product in a good yield was accomplished using Pd(II)@(BPyDC)_{*x*%}-ETTA COFs (*x* = 25%, 50%, 75%, 100%) in comparison to pristine COFs (Table 2, entry 1–6). Conversion of C–H to C–Cl using *N*-chlorosuccinimide (NCS) was achieved in good (76%) yield, whereas, C–I conversion using *N*-iodosuccinimide (NIS) as oxidant was unsuccessful. This is probably due to steric constraints of planar substrate as illustrated in Table 2 (entry 8, 9). These observations illustrated the role of active Pd(II) moieties in the bipyridine functionalized COFs and increase in the palladium content is directly proportional to percentage yield of C–H functionalized product. As highlighted in Table 1, Pd(II)@(BPyDC)_{25%}-ETTA, Pd(II)@(BPyDC)_{50%}-ETTA, Pd(II)@(BPyDC)_{75%}-ETTA, and Pd(II)@(BPyDC)_{100%}-ETTA COFs showed C–H to C–OMe conversion in 21%, 49%, 71%, and 86% yield, respectively. Reusability and recyclability are essential for heterogeneous catalysis, particularly in industrial applications. Pd(II)@(BPyDC)_{100%}-ETTA COF exhibited good reusability that can be recovered by filtration. After recycling four times, catalytic activity toward the hierarchical C–H to C–OCH₃ and C–Br functionalization was slightly declined as a result of partial blockage of pore channels after every

Table 2. Regioselective C–H to C–X (X = Br, Cl, I) functionalization of benzo[*h*]quinoline using homogeneous and heterogeneous catalysts.



Entry	Halogenating agent (NXS)	Catalyst	Yield ^{a)} [%]
1	NBS	Blank	0
2 ^{b)}	NBS	100%-ETTA-BPyDC	<5
3 ^{b)}	NBS	Pd(II)@25%-ETTA-BPyDC	14
4 ^{b)}	NBS	Pd(II)@50%-ETTA-BPyDC	31
5 ^{b)}	NBS	Pd(II)@75%-ETTA-BPyDC	69
6 ^{b)}	NBS	Pd(II)@100%-ETTA-BPyDC	80
7 ^{b)}	NBS	Pd(OAc) ₂	92
8 ^{b)}	NCS	Pd(II)@100%-ETTA-BPyDC	76
9 ^{b)}	NIS	Pd(II)@100%-ETTA-BPyDC	27

^{a)}Determined by ¹H-NMR; ^{b)}0.05 mmol of substrate, 0.075 mmol of NXS, catalyst (100 mg), and 2.0 mL of CH₃CN.

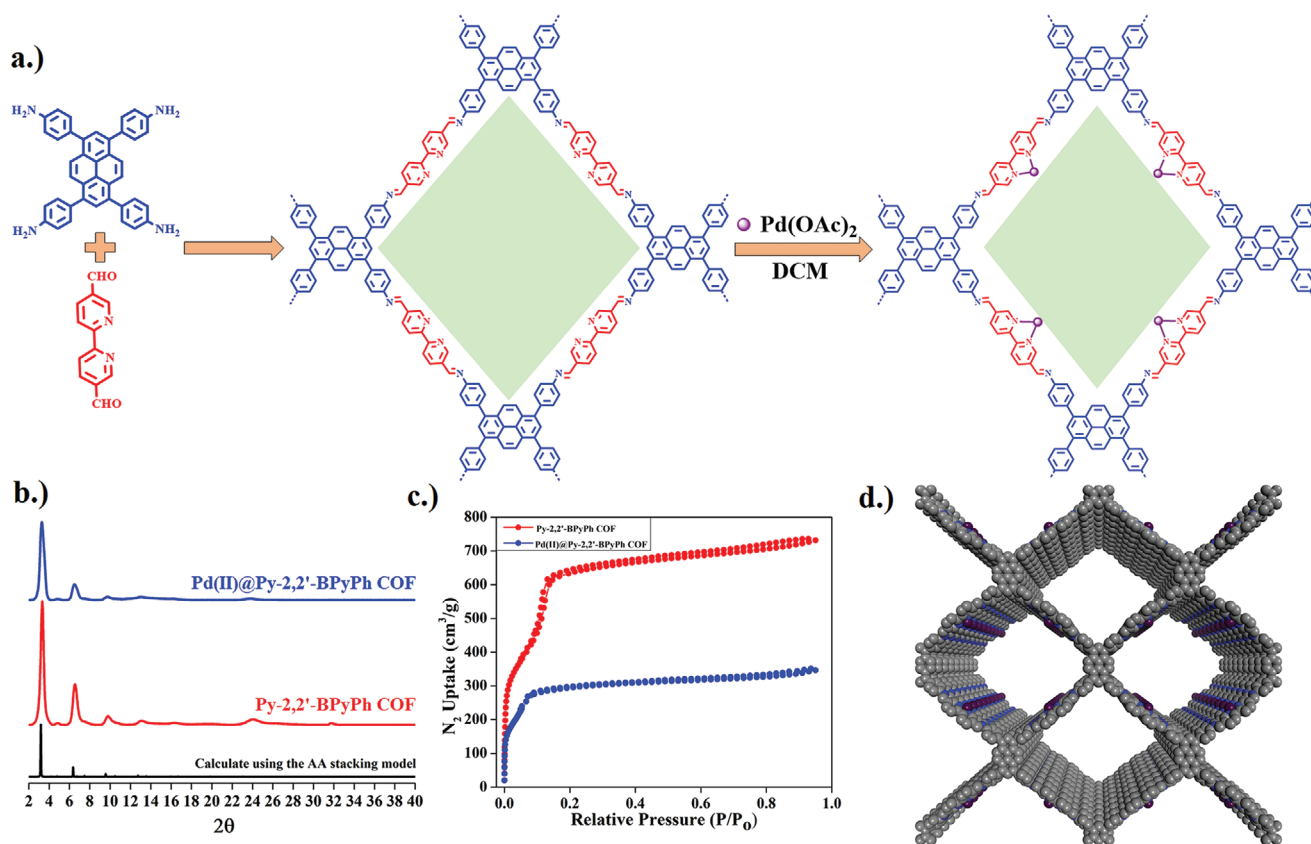


Figure 3. a) Synthetic scheme of Py-2,2'-BPyPh COF and Pd(II)@Py-2,2'-BPyPh COF. b) Calculated and experimental PXRD pattern of Py-2,2'-BPyPh COF and Pd(II)@Py-2,2'-BPyPh COF. c) N₂ sorption isotherms collected at 77 K. d) Graphic extended view of AA-stacking mode of Pd(II)@Py-2,2'-BPyPh COF.

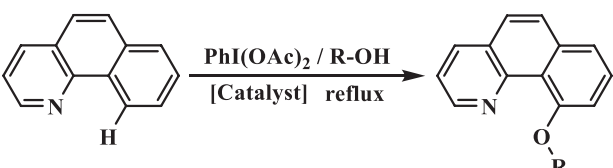
reaction, as evident in the decrease of surface area (Figure S15, Supporting Information). In addition, the complete retention of PXRD pattern, FTIR analysis, and EPR spectrum verified the immobilized framework stability in context of crystallinity, –CN functionalities, and palladium docking, respectively (Figures S16–S19, Supporting Information).

To distinctly analyze the influence of the core properties, including pore structure of the frameworks as decorating platform for palladium to explore C–H to C–O and C–Br functionalization, side-by-side comparisons were made with the palladium immobilized single-pore bipyridine functionalized COF bearing uniform pore structure and pore environment to the mesopore in (BPyDC)_{x%}-ETTA framework. Py-2,2'-BPyPh COF is synthesized by condensation of 4,4',4'',4'''-(pyrene-1,3,6,8-tetrayl)tetraaniline (PyTTA) and 2,2'-BPyDCA in the presence of acetic acid followed by palladium immobilization as described in Figure 3a, and referred as Pd(II)@Py-2,2'-BPyPh COF. PXRD pattern together with pore size and surface area measurements revealed that immobilized framework has high crystallinity and square channel (Figure 3b–d and Figure S20, Supporting Information). The BET and Langmuir surface area of pristine Py-2,2'-BPyPh framework were 1784 m² g⁻¹ and 2746 m² g⁻¹, which was reduced to 1023 m² g⁻¹ and 1360 m² g⁻¹ after palladium docking (9.3 wt%), respectively. FTIR, ¹³C MAS NMR, TGA, and SEM measurements were implemented to probe –C=N moieties, thermostability, and morphology of the prepared frameworks as shown in Figures S21–S24 (Supporting Information). XPS

spectrum of Pd(II)@Py-2,2'-BPyPh COF (Figure S25, Supporting Information) exhibited the binding energies of Pd 3d_{3/2} and 3d_{5/2} peak at 343.4 and 337.9 eV, respectively, along with the blueshifted N1s from 398.1 eV in pristine framework to 399.6 eV suggesting the strong interaction between bipyridine moieties and Pd(II) in the modified framework. Thus, even though the pore channel of single-pore framework is partially occupied by palladium, the surface area is still sufficient enough to ingress and egress of molecule with access of metal sites.

As displayed in Table 1, the catalytic activity of (BPyDC)_{x%}-ETTA (x = 0%, 25%, 50%, 75%, 100%), Pd(II)@(BPyDC)_{x%}-ETTA (x = 25%, 50%, 75%, 100%) frameworks afforded low-to-moderate C–H to C–O, C–X (X = Br, Cl) functionalization yield. The fact that single-pore frameworks also act as a decorating platform with high surface area, pore volume, and pore environment, it suggests the profound role of the architecture in C–H functionalization activity. To further gain an insight for C–H functionalization, single-pore Py-2,2'-BPyPh and Pd(II)@Py-2,2'-BPyPh frameworks were also employed. The percentage conversion of benzo[h]quinoline to 10-methoxybenzo[h]quinoline using pristine Py-2,2'-BPyPh COF afford <5% conversion. However, the single-pore Pd(II)@Py-2,2'-BPyPh led to 92% yield for same catalytic reaction (Table 3, entry 3). To confirm the nature of heterogeneity, hot filtration tests were performed after 24 h and removing the Pd(II)@Py-2,2'-BPyPh framework led to almost no C–H to C–Br and C–OMe functionalization as shown in Figure S26 (Supporting Information). This finding illustrates the

Table 3. Dual-pore and single-pore palladium docked framework catalyzed regioselective alkoxy group instalment of benzo[*h*]quinoline.



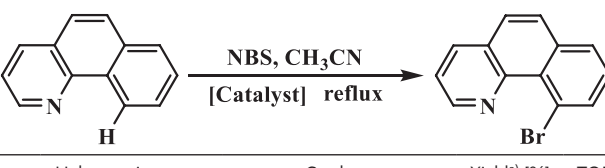
Entry	R (product/solvent)	Catalysts	Yield ^{a)} [%]	TON ^{b)}
1 ^{c)}	CH ₃	Pd(II)@100%-ETTA-BPyDC	86	76
2 ^{c)}	CH ₂ CH ₃	Pd(II)@100%-ETTA-BPyDC	72	66
3 ^{c)}	CH ₃	Pd(II)@Py-2,2'-BPyPh	92	53
4 ^{c)}	CH ₂ CH ₃	Pd(II)@Py-2,2'-BPyPh	83	47

^{a)}Determined by ¹H-NMR; ^{b)}TON is number of moles of benzo[*h*]quinoline converted to methoxy product per mole of palladium present in catalyst; ^{c)}0.05 mmol of substrate, 0.125 mmol of PhI(OAc)₂, catalyst (100 mg), and 2.0 mL of alcohol (R–OH).

principle of heterogeneity and role of palladation in the bipyridine decorated frameworks. Furthermore, the structure integrity of Pd(II)@Py-2,2'-BPyPh framework after C–H functionalization was examined by PXRD and surface area analysis (Figures S27 and S28, Supporting Information). PXRD pattern of recyclable Pd(II)@Py-2,2'-BPyPh exhibited strong peak at 3.3° corresponding to (110) facet, similar to the pristine framework. The BET surface area measurement of recyclable Pd(II)@Py-2,2'-BPyPh COF after C–H to C–Br and C–OMe functionalization is 710 and 849 m² g⁻¹, respectively, comparable to palladium docked single-pore pristine framework (1023 m² g⁻¹).

To provide a comprehensive comparison, the single-pore Pd(II)@Py-2,2'-BPyPh COF efficiently installed alkoxy group (–OCH₂CH₃) at C₁₀ position of benzo[*h*]quinoline in quantitative yield. On the other hand, lower yield is observed for 1-butanol due to weak nucleophilicity. A plausible mechanism for C–H oxygenation using palladium docked frameworks is outlined in Figure S29 (Supporting Information). The reaction occurs initially via generation of cyclopalladated intermediate upon treatment of Pd(II) with benzo[*h*]quinoline, followed by a two-electron oxidation of the palladacycle using PhI(OAc)₂ as an oxidant to generate Pd(IV) species. Finally, the C–OR bond is formed by reductive elimination that leads to product release with regeneration of catalyst.^[15,90] Notably, the high regioselectivity of the catalytic reaction arose from the reactive cyclopalladated complex at C₁₀ position of benzo[*h*]quinoline, which in turn, provides evidence for C₁₀–H functionalized product. In addition to this, chelate-directed oxidation can be prolonged to *N*-bromosuccinimide as both oxidants and halogenating reagents to establish the structure–function relationship in C–H to C–Br conversion. The conversion of benzo[*h*]quinoline to 10-bromobenzo[*h*]quinoline using either dual-pore Pd(II)@[(BPyDC)]_{100%}-ETTA or single-pore Pd(II)@Py-2,2'-BPyPh COF afforded 80% and 91% yield, respectively (Table 4), which are comparable to homogeneous Pd(OAc)₂ catalyst. The turnover number (TON) for C–H functionalization in the presence of dual-pore and single-pore docked catalyst was compared (Tables 3 and 4), which in turn unambiguously suggested the profound role of metal docking, pore volume, and stability in heterogeneous catalytic reactions. After such encouraging results and comparisons, we

Table 4. Dual-pore and single-pore palladium docked framework catalyzed C–H bond halogenation reactions.



Entry	Halogenating agent	Catalysts	Yield ^{a)} [%]	TON ^{b)}
1 ^{c)}	NBS	Pd(II)@100%-ETTA-BPyDC	80	71
2 ^{c)}	NBS	Pd(II)@Py-2,2'-BPyPh	91	52
3 ^{c)}	NBS	Pd(OAc) ₂	92	

^{a)}Determined by ¹H-NMR; ^{b)}TON is number of moles of benzo[*h*]quinoline converted to bromo product per mole of palladium present in catalyst; ^{c)}0.05 mmol of substrate, 0.75 mmol of NBS, catalyst (100 mg), and 2.0 mL of CH₃CN.

underlined that the dual-pore Pd(II)@[(BPyDC)]_{100%}-ETTA and single-pore Pd(II)@Py-2,2'-BPyPh COF exhibited significant catalytic activity for C–H functionalization. The enhanced catalytic activity of Pd(II)@[(BPyDC)]_{100%}-ETTA as compared to Pd(II)@Py-2,2'-BPyPh COF is prone to higher degree of active sites and the importance of pore structure in facilitating the diffusion of reactants/products thereby avoiding clogging and increasing the durability/lifetime of catalyst,^[92] which is of significant importance in using porous materials as scaffold for various applications including catalysis.

3. Conclusion

In summary, we have successfully demonstrated the facile synthesis of imine-linked dual-pore [(BPyDC)]_{*x*%}-ETTA COFs (*x* = 0%, 25%, 50%, 75%, 100%) with controllable bipyridine contents as a viable decorating platform for palladium immobilization. The immobilized Pd(II)@[(BPyDC)]_{*x*%}-ETTA dual-pore frameworks with varying palladium content are characterized by using various analytical techniques, and utilized as highly efficient heterogeneous catalyst for selective C–H functionalization to C–X (X = Br, Cl) and C–OR (R = Me, Et) with excellent reusability and recyclability. Significantly, the catalytic activity of palladium immobilized dual-pore Pd(II)@[(BPyDC)]_{*x*%}-ETTA frameworks was compared favorably over the single-pore imine-linked Pd(II)@Py-2,2'-BPyDC framework presumably due to the facilitated diffusion of reactants/products. To the best of our knowledge, the palladium docked dual-pore and single-pore COFs presented herein are the first investigated example for selective C–H functionalization. These sporadic examples of chelation-assisted C–H functionalization emphasized the structure–function relationship of COFs and provide an overview of fine-tuning of core properties of existed or novel frameworks for key organic and organometallic conversions.

4. Experimental Section

Reagents: All the reagents and solvents were purchased from commercial sources and used as received without any further purification. Pyrene (Acros Organics, ≥97.5%), palladium

tetrakis(triphenylphosphine) (Sigma-Aldrich, 99%), tetraphenylethene (Alfa Aesar, 98%), 4-bromobenzaldehyde (Sigma-Aldrich, 99%), 4-(4,4,5,5-tetramethyl-1,3,4-dioxaborolan-2-yl)aniline (Oakwood Chemical, 98%), 4-formylphenylboronic acid (Matrix Scientific, 97%), potassium carbonate (Sigma-Aldrich, 99%), 5,5'-dimethyl-2,2'-bipyridine (Alfa Aesar, 98%), *N*-bromosuccinimide (Oakwood Chemical, 99%), hexamethylenetetramine (Acros Organics, 99%), hydrazine monohydrate (TCI America, ≥98%), palladium acetate (Acros Organics), 10% Pd/C (TCI America), hydrochloric acid (Sigma-Aldrich, ACS grade), acetic acid (Sigma-Aldrich), fuming nitric acid (Sigma-Aldrich), dichloromethane (Sigma-Aldrich), ethanol (Sigma-Aldrich), chloroform (Acros Organics), acetonitrile (Sigma-Aldrich), and tetrahydrofuran (Acros Organics) were used as received. PyTTA,^[91] ETTA,^[92] 2,2'-BPyDCA,^[93] 4,4'-BPhDCA,^[94] and Py-2,2'-BPyPh COF^[95] were synthesized as per the reported procedures.

Synthesis of [(BPyDC)]_{25%}-ETTA COFs: A Pyrex tube with o.d. × i.d. = 9.5 mm × 7.5 mm was charged with 4,4',4'',4'''-(ethene-1,1,2,2-tetra)l)tetraaniline (0.0764 mmol, 30 mg), 2,2'-BPyDCA (*X* = 25% (8.11 mg)), and 4,4'-BPhDCA (*X* = 75% (24.11 mg)) in a mixture of 1,4-dioxane (1 mL) and 6 M acetic acid (0.1 mL). The tube was flash frozen at 77 K using liquid N₂ bath for 5 min, evacuated and flame sealed. The reaction mixture was heated at 120 °C without disturbance for 3 d to afford red solid, which was isolated by filtration and washed with copious amount of dry tetrahydrofuran and dry acetone. The yellow fluffy powder was dried at 120 °C under vacuum for 12 h before subjected to any characterization. Similar procedure was used to prepare [(BPyDC)]_{*x%*}-ETTA COFs (*x* = 0%, 50%, 75%, 100%) except the amount of 2,2'-BPyDCA (*X* = 0% (0 mg), 50% (16.22 mg), 75% (24.33 mg), 100% (32.44 mg)) and 4,4'-BPhDCA (*X* = 0% (0 mg), 25% (8.04 mg), 50% (16.07 mg), 100% (32.14 mg)).

Synthesis of Pd(II)@[(BPyDC)]_{*x%*}-ETTA COFs: In a typical procedure, [(BPyDC)]_{*x%*}-ETTA COFs (0.04 mmol) was reacted with a solution of Pd(OAc)₂ in dichloromethane (5 mL). The resulting suspension was stirred overnight at ambient temperature. The resulting solid was filtered, washed with excess of dichloromethane to remove unbound metal salt, and then dried under vacuum for 12 h.

Similar procedure was performed to successfully synthesize Pd(II)@Py-2,2'-BPyPh COF except the amount of Pd(OAc)₂ in dichloromethane.

Catalytic Tests: Catalysis of Alkoxy Group Installation on Benzo[*h*]quinoline: Under inert condition, benzo[*h*]quinoline (0.05 mmol, 10 mg), (diacetoxyiodo)benzene (PhI(OAc)₂, 0.125 mmol, 40 mg), and 2 mL of the solvent (MeOH, EtOH, *n*-PrOH, and catalysts listed in Tables 1 and 3) were charged in a 10 mL Schlenk tube. The mixture was refluxed for 48 h. After cooling down, the supernatant was collected and analyzed by ¹H-NMR using CDCl₃. To test the recyclability, the solid recovered catalyst was washed with copious amount of alcohol solvent followed by dichloromethane and dried under vacuum before using for next catalytic cycle.

Catalytic Tests: Catalysis of C–H Bond Halogenation Reactions: Benzo[*h*]quinoline (0.05 mmol, 10 mg), *N*-bromosuccinimide (0.075 mmol, 14 mg), 2 mL of acetonitrile, and catalysts listed in Tables 2 and 4 were added to a 10 mL Schlenk tube. The mixture was heated at 85 °C for 48 h. After cooling the solution at room temperature, the supernatant was identified by ¹H-NMR. To test the recyclability, the solid recovered catalyst was washed with acetonitrile, dichloromethane, and dried under vacuum before using for next C–H bond halogenation reaction.

Supporting Information

Supporting Information is available from the Wiley Online Library or from the author.

Acknowledgements

The authors acknowledge the Distinguished Scientist Fellowship Program (DSFP) at King Saud University (SM/AMA) for support of this

work. Partial support from the Robert A. Welch Foundation (B-0027) is also acknowledged (S.M.). X-ray photoelectron spectroscopy studies were carried in the Nebraska Nanoscale Facility, Nebraska Center for Materials and Nanoscience, which was supported by the NSF under award NNCI Grant No. 1542182, and the Nebraska Research Initiatives (NRI).

Conflict of Interest

The authors declare no conflict of interest.

Keywords

C–H functionalization, covalent–organic frameworks, heterogeneous catalysis, palladium, pore surface engineering

Received: July 1, 2020

Revised: August 5, 2020

Published online: September 11, 2020

- [1] L. Ackermann, *Chem. Rev.* **2011**, *111*, 1315.
- [2] F. Kakiuchi, S. Murai, *Acc. Chem. Res.* **2002**, *35*, 826.
- [3] V. Ritleng, C. Sirlin, M. Pfeffer, *Chem. Rev.* **2002**, *102*, 1731.
- [4] R. A. Periana, O. Mironov, D. Taube, G. Bhalla, C. J. Jones, *Science* **2003**, *301*, 814.
- [5] S. Mukhopadhyay, A. T. Bell, *Angew. Chem., Int. Ed.* **2003**, *42*, 2990.
- [6] R. A. Periana, D. J. Taube, S. Gamble, H. Taube, T. Satoh, H. Fujii, *Science* **1998**, *280*, 560.
- [7] B. D. Dangel, J. A. Johnson, D. Sames, *J. Am. Chem. Soc.* **2001**, *123*, 8149.
- [8] H. Chen, S. Schlecht, T. S. Semple, J. F. Hartwig, *Science* **2000**, *287*, 1995.
- [9] H. M. L. Davies, R. E. J. Beckwith, *Chem. Rev.* **2003**, *103*, 2861.
- [10] J. J. Li, D. S. Johnson, *Modern Drug Synthesis*, Wiley, Hoboken, NJ **2010**.
- [11] S. Enthaler, A. Company, *Chem. Soc. Rev.* **2011**, *40*, 4912.
- [12] J. Yamaguchi, A. D. Yamaguchi, K. Itami, *Angew. Chem., Int. Ed.* **2012**, *51*, 8960.
- [13] L. V. Desai, K. L. Hull, M. S. Sanford, *J. Am. Chem. Soc.* **2004**, *126*, 9542.
- [14] D. Kalyani, A. R. Dick, W. Q. Anani, M. S. Sanford, *Tetrahedron* **2006**, *62*, 11483.
- [15] T. W. Lyons, M. S. Sanford, *Chem. Rev.* **2010**, *110*, 1147.
- [16] S. Y. Zhang, G. He, W. A. Nack, Y. Zhao, Q. Li, G. Chen, *J. Am. Chem. Soc.* **2013**, *135*, 2124.
- [17] Q. Zhang, K. Chen, W. Rao, Y. Zhang, F. J. Chen, B. F. Shi, *Angew. Chem., Int. Ed.* **2013**, *52*, 13588.
- [18] A. R. Dick, K. L. Hull, M. S. Sanford, *J. Am. Chem. Soc.* **2004**, *126*, 2300.
- [19] X. Zhao, E. Dimitrijević, V. M. Dong, *J. Am. Chem. Soc.* **2009**, *131*, 3466.
- [20] K. L. Hull, W. Q. Anani, M. S. Sanford, *J. Am. Chem. Soc.* **2006**, *128*, 7134.
- [21] O. Daugulis, V. G. Zaitsev, *Angew. Chem., Int. Ed.* **2005**, *44*, 4046.
- [22] K. L. Hull, E. L. Lanni, M. S. Sanford, *J. Am. Chem. Soc.* **2006**, *128*, 14047.
- [23] W.-Y. Yu, W. N. Sit, K.-M. Lai, Z. Zhou, A. S. C. Chan, *J. Am. Chem. Soc.* **2008**, *130*, 3304.
- [24] K. Geng, T. He, R. Liu, S. Dalapati, K. T. Tan, Z. Li, S. Tao, Y. Gong, Q. Jiang, D. Jiang, *Chem. Rev.* **2020**, <https://doi.org/10.1021/acs.chemrev.9b00550>.

- [25] H. Lyu, C. S. Diercks, C. Zhu, O. M. Yaghi, *J. Am. Chem. Soc.* **2019**, *141*, 6848.
- [26] A. Acharjya, P. Pachfule, J. Roesner, F.-J. Schmitt, A. Thomas, *Angew. Chem., Int. Ed.* **2019**, *58*, 14865.
- [27] S.-Y. Jiang, S.-X. Gan, X. Zhang, H. Li, Q.-Y. Qi, F.-Z. Cui, J. Lu, X. Zhao, *J. Am. Chem. Soc.* **2019**, *141*, 14981.
- [28] Y. Liu, C. S. Diercks, Y. Ma, H. Lyu, C. Zhu, S. A. Alshimiri, S. Alshihri, O. M. Yaghi, *J. Am. Chem. Soc.* **2019**, *141*, 677.
- [29] B. Zhang, H. Mao, R. Matheu, J. A. Reimer, S. A. Alshimiri, S. Alshihri, O. M. Yaghi, *J. Am. Chem. Soc.* **2019**, *141*, 11420.
- [30] H. L. Nguyen, C. Gropp, O. M. Yaghi, *J. Am. Chem. Soc.* **2020**, *142*, 2771.
- [31] R.-R. Liang, S.-Y. Jiang, A. Ru-Han, X. Zhao, *Chem. Soc. Rev.* **2020**, *49*, 3920.
- [32] C. Qian, Q.-Y. Qi, G.-F. Jiang, F.-Z. Cui, Y. Tian, X. Zhao, *J. Am. Chem. Soc.* **2017**, *139*, 6736.
- [33] Y. Zhai, G. Liu, F. Jin, Y. Zhang, X. Gong, Z. Miao, J. Li, M. Zhang, Y. Cui, L. Zhang, Y. Liu, H. Zhang, Y. Zhao, Y. Zeng, *Angew. Chem., Int. Ed.* **2019**, *58*, 17679.
- [34] Z.-F. Pang, T.-Y. Zhou, R.-R. Liang, Q.-Y. Qi, X. Zhao, *Chem. Sci.* **2017**, *8*, 3866.
- [35] Q. Sun, B. Aguila, J. A. Perman, N. Nguyen, S. Ma, *J. Am. Chem. Soc.* **2016**, *138*, 15790.
- [36] X. Wang, X. Han, J. Zhang, X. Wu, Y. Liu, Y. Cui, *J. Am. Chem. Soc.* **2016**, *138*, 12332.
- [37] S. Lu, Y. Hu, S. Wan, R. McCaffrey, Y. Jin, H. Gu, W. Zhang, *J. Am. Chem. Soc.* **2017**, *139*, 17082.
- [38] H. Liu, J. Chu, Z. Yin, X. Cai, L. Zhuang, H. Deng, *Chem* **2018**, *4*, 1696.
- [39] J. Roeser, T. Langenhahn, M. Schwarze, R. Schomäcker, A. Thomas, J. Schmidt, *J. Am. Chem. Soc.* **2018**, *140*, 1423.
- [40] Y. Du, H. Yang, J. M. Whiteley, S. Wan, Y. Jin, S.-H. Lee, W. Zhang, *Angew. Chem., Int. Ed.* **2016**, *55*, 1737.
- [41] Z. Wang, S. Zhang, Y. Chen, Z. Zhang, S. Ma, *Chem. Soc. Rev.* **2020**, *49*, 708.
- [42] Y. Zeng, R. Zou, Y. Zhao, *Adv. Mater.* **2016**, *28*, 2855.
- [43] A. Baldwin, J. W. Crowe, D. A. Pyles, P. L. McGrier, *J. Am. Chem. Soc.* **2016**, *138*, 15134.
- [44] Y. Pramudya, J. L. Mendoza-Cortes, *J. Am. Chem. Soc.* **2016**, *138*, 15204.
- [45] Y. Yang, M. Faheem, L. Wang, Q. Meng, H. Sha, N. Yang, Y. Yuan, G. Zhu, *ACS Cent. Sci.* **2018**, *4*, 748.
- [46] Q. Sun, B. Aguila, J. Perman, L. Earl, C. Abney, Y. Cheng, H. Wei, N. Nguyen, L. Wojtas, S. Ma, *J. Am. Chem. Soc.* **2017**, *139*, 2786.
- [47] Q. Sun, B. Aguila, Y. Song, S. Ma, *Acc. Chem. Res.* **2020**, *53*, 812.
- [48] Z. Li, H. Li, X. Guan, J. Tang, Y. Yusran, Z. Li, M. Xue, Q. Fang, Y. Yan, V. Valtchev, S. Qiu, *J. Am. Chem. Soc.* **2017**, *139*, 17771.
- [49] G. H. V. Bertrand, V. K. Michaelis, T.-C. Ong, R. G. Griffin, M. Dincă, *Proc. Natl. Acad. Sci. USA* **2013**, *110*, 4923.
- [50] M. Calik, F. Auras, L. M. Salonen, K. Bader, I. Grill, M. Handloser, D. D. Medina, M. Dogru, F. Löbermann, D. Trauner, A. Hartschuh, T. Bein, *J. Am. Chem. Soc.* **2014**, *136*, 17802.
- [51] L. Chen, K. Furukawa, J. Gao, A. Nagai, T. Nakamura, Y. Dong, D. Jiang, *J. Am. Chem. Soc.* **2014**, *136*, 9806.
- [52] J. Xu, Y. He, S. Bi, M. Wang, P. Yang, D. Wu, J. Wang, F. Zhang, *Angew. Chem., Int. Ed.* **2019**, *131*, 12193.
- [53] C. R. DeBlase, K. E. Silverstein, T. T. Truong, H. D. Abruna, W. R. Dichtel, *J. Am. Chem. Soc.* **2013**, *135*, 16821.
- [54] S. Wang, Q. Wang, P. Shao, Y. Han, X. Gao, L. Ma, S. Yuan, X. Ma, J. Zhou, X. Feng, B. Wang, *J. Am. Chem. Soc.* **2017**, *139*, 4258.
- [55] B.-Y. Lu, Z.-Q. Wang, F.-Z. Cui, J.-Y. Li, X. Han, Q.-Y. Qi, D.-L. Ma, G.-F. Jiang, X.-X. Zeng, X. Zhao, *ACS Appl. Mater. Interfaces* **2020**, *12*, 34990.
- [56] S. Kandambeth, V. Venkatesh, D. B. Shinde, S. Kumari, A. Halder, S. Verma, R. Banerjee, *Nat. Commun.* **2015**, *6*, 6786.
- [57] Y. Peng, Y. Huang, Y. Zhu, B. Chen, L. Wang, Z. Lai, Z. Zhang, M. Zhao, C. Tan, N. Yang, F. Shao, Y. Han, H. Zhang, *J. Am. Chem. Soc.* **2017**, *139*, 8698.
- [58] Q. Sun, C.-W. Fu, B. Aguila, J. A. Perman, S. Wang, H.-Y. Huang, F.-S. Xiao, S. Ma, *J. Am. Chem. Soc.* **2018**, *140*, 984.
- [59] H. L. Nguyen, N. Hanikel, S. J. Lyle, C. Zhu, D. M. Proserpio, O. M. Yaghi, *J. Am. Chem. Soc.* **2020**, *142*, 2218.
- [60] F.-Z. Cui, J.-J. Xie, S.-Y. Jiang, S.-X. Gan, D.-L. Ma, R.-R. Liang, G.-F. Jiang, X. Zhao, *Chem. Commun.* **2019**, *55*, 4550.
- [61] H. Vardhan, G. Verma, S. Ramani, A. Nafady, A. M. Al-Enizi, Y. Pan, Z. Yang, S. Ma, *ACS Appl. Mater. Interfaces* **2019**, *11*, 3070.
- [62] H. Vardhan, L. Hou, E. Yee, A. Nafady, M. A. Al-Abdrabalnabi, A. M. Al-Enizi, Y. Pan, Z. Yang, S. Ma, *ACS Sustainable Chem. Eng.* **2019**, *7*, 4878.
- [63] H. Vardhan, Y. Pan, Z. Yang, G. Verma, A. Nafady, A. M. Al-Enizi, T. M. Alotaibi, O. A. Almaghrabi, S. Ma, *APL Mater.* **2019**, *7*, 101111.
- [64] L. A. Baldwin, J. W. Crowe, D. A. Pyles, P. L. McGrier, *J. Am. Chem. Soc.* **2016**, *138*, 15134.
- [65] W. K. Haug, E. R. Wolfson, B. T. Morman, C. M. Thomas, P. L. McGrier, *J. Am. Chem. Soc.* **2020**, *142*, 5521.
- [66] W. Leng, Y. Peng, J. Zhang, H. Lu, X. Feng, R. Ge, B. Dong, B. Wang, X. Hu, Y. Gao, *Chem. - Eur. J.* **2016**, *22*, 9087.
- [67] Y. Zhao, W. Dai, Y. Peng, Z. Niu, Q. Sun, C. Shan, Y. Hang, L. Wojtas, D. Yuan, Z. Zhang, H. Dong, X. Zhang, B. Zhang, Y. Feng, S. Ma, *Angew. Chem., Int. Ed.* **2020**, *59*, 4354.
- [68] L.-H. Li, X.-L. Feng, X.-H. Cui, Y.-X. Ma, S.-Y. Ding, W. Wang, *J. Am. Chem. Soc.* **2017**, *139*, 6042.
- [69] W. Zhang, P. Jiang, Y. Wang, J. Zhang, Y. Gao, P. Zhang, *RSC Adv.* **2014**, *4*, 51544.
- [70] T. Kundu, J. Wang, Y. Cheng, Y. Du, Y. Qian, G. Liu, D. Zhao, *Dalton Trans.* **2018**, *47*, 13824.
- [71] J. L. Segura, S. Royuela, M. M. Ramos, *Chem. Soc. Rev.* **2019**, *48*, 3903.
- [72] H. Vardhan, A. Nafady, A. M. Al-Enizi, S. Ma, *Nanoscale* **2019**, *11*, 21679.
- [73] P. J. Waller, Y. S. AlFaraj, C. S. Diercks, N. N. Jarenwattananon, O. M. Yaghi, *J. Am. Chem. Soc.* **2018**, *140*, 9099.
- [74] S. J. Lyle, T. M. Osborn Popp, P. J. Waller, X. Pei, J. A. Reimer, O. M. Yaghi, *J. Am. Chem. Soc.* **2019**, *141*, 11253.
- [75] L. Guo, S. Jia, C. S. Diercks, X. Yang, S. A. Alshimiri, O. M. Yaghi, *Angew. Chem., Int. Ed.* **2020**, *59*, 2023.
- [76] M. Bhadra, S. Kandambeth, M. K. Sahoo, M. Addicoat, E. Balaraman, R. Banerjee, *J. Am. Chem. Soc.* **2019**, *141*, 6152.
- [77] M. Bhadra, H. S. Sasmal, A. Basu, S. P. Midya, S. Kandambeth, P. Pachfule, E. Balaraman, R. Banerjee, *ACS Appl. Mater. Interfaces* **2017**, *9*, 13785.
- [78] D. B. Shinde, S. Kandambeth, P. Pachfule, R. R. Kumar, R. Banerjee, *Chem. Commun.* **2015**, *51*, 310.
- [79] C. S. Diercks, S. Lin, N. Kornienko, E. A. Kapustin, E. M. Nichols, C. Zhu, Y. Zhao, C. J. Chang, O. M. Yaghi, *J. Am. Chem. Soc.* **2018**, *140*, 1116.
- [80] D. A. Popov, J. M. Luna, N. M. Orchanian, R. Haiges, C. A. Downes, S. C. Marinescu, *Dalton Trans.* **2018**, *47*, 17450.
- [81] E. M. Johnson, R. Haiges, S. C. Marinescu, *ACS Appl. Mater. Interfaces* **2018**, *10*, 37919.
- [82] X. Li, Z. Wang, J. Sun, J. Gao, Y. Zhao, P. Cheng, B. Aguila, S. Ma, Y. Chen, Z. Zhang, *Chem. Commun.* **2019**, *55*, 5423.
- [83] D.-X. Zhang, J. Liu, H.-X. Zhang, T. Wen, J. Zhang, *Inorg. Chem.* **2015**, *54*, 6069.
- [84] B. Morzyk, D. Michalska, M. K. Marchewka, *J. Coord. Chem.* **1999**, *47*, 241.
- [85] Y. B. Dudkina, K. V. Kholin, T. V. Gryaznova, D. R. Islamov, O. N. Kataeva, I. Rizvanov, A. I. Levitskaya, O. D. Fominykh, M. Y. Balakina, O. G. Sinyashin, Y. H. Budnikova, *Dalton Trans.* **2017**, *46*, 165.

- [86] F. Xu, H. Xu, X. Chen, D. Wu, Y. Wu, H. Liu, C. Gu, R. Fu, D. Jiang, *Angew. Chem., Int. Ed.* **2015**, *54*, 6814.
- [87] V. Snieckus, *Chem. Rev.* **1990**, *90*, 879.
- [88] G. K. S. Prakash, T. Mathew, D. Hoole, P. M. Esteves, Q. Wang, G. Rasul, G. A. Olah, *J. Am. Chem. Soc.* **2004**, *126*, 15770.
- [89] D. Gimenez, A. Dose, N. L. Robson, G. Sandford, S. L. Cobb, C. R. Coxon, *Org. Biomol. Chem.* **2017**, *15*, 4081.
- [90] S. R. Neufeldt, M. S. Sanford, *Acc. Chem. Res.* **2012**, *45*, 936.
- [91] N. Huang, P. Wang, M. A. Addicoat, T. Heine, D. Jiang, *Angew. Chem., Int. Ed.* **2017**, *56*, 4982.
- [92] Q. Sun, B. Aguila, P. C. Lan, S. Ma, *Adv. Mater.* **2019**, *31*, 1900008.
- [93] J. Hodačová, M. Buděšínský, *Org. Lett.* **2007**, *9*, 5641.
- [94] J. Jayabharathi, A. Prabhakaran, V. Thanikachalam, P. Jeeva, *New J. Chem.* **2016**, *40*, 8768.
- [95] X. Chen, N. Huang, J. Gao, H. Xu, F. Xu, D. Jiang, *Chem. Commun.* **2014**, *50*, 6161.